16th European Signal Processing Conference (EUSIPCO 2008), Lausanne, Switzerland, August 25-29, 2008, copyright by EURASIP

STATISTICAL IMAGE MODELING USING DISTRIBUTION OF RELATIVE PHASE IN THE COMPLEX WAVELET DOMAIN

An Vo, Soontorn Oraintara and Truong T. Nguyen

Department of Electrical Engineering, University of Texas Arlington, TX 76019, USA, and
Geophysic Research Center, Paris School of Mines, Fontainebleau, 77305 France,
E-mail: vpnan@msp.uta.edu, oraintar@uta.edu, truong.nguyen@ensmp.fr

ABSTRACT

In this paper, the probability density function of relative phase (fRP) is proposed for modeling natural images in the transform domain. We demonstrate that the fRP fits well with the behaviors of relative phase in the complex directional wavelet subband from different natural images. Moreover, a new image feature based on the fRP is proposed for texture image retrieval application. The fRP based feature yields a higher retrieval accuracy compared to the energy features, the relative phase features and the generalized Gaussian density based features (GGD). In addition to the GGD based features, the fRP phase information is also incorporated to further improve the performance.

1. INTRODUCTION

Many applications in image processing such as image compression, denoising or retrieval can benefit from a statistical model to characterize the image in the transform domain. A clean, precise probability model which can sufficiently describe typical images becomes essential. In this paper, a new model for relative phase of the complex directional wavelet coefficients is proposed for image modeling, and its application in the texture image retrieval is presented.

There are many works on the statistics of decomposition coefficients of the wavelet transform [1]. The wavelet coefficients within a subband were often assumed to be independent and identically distributed. With this assumption, the wavelet coefficients can be modeled by the marginal model whose distribution is a two-parameter generalized Gaussian density (GGD). The GGD is a suitable distribution for the peaky and heavy-tailed non-Gaussian statistic of typical image wavelet decomposition. A number of researchers have successfully developed joint statistical models in the wavelet domain [2][3]. The hidden Markov tree was introduced in [2] to model the wavelet decomposition. A bivariate probability density function has been proposed to model the statistical dependencies between a wavelet coefficient and its parent [4]. In [3], the authors developed a model for the neighborhoods of oriented pyramid coefficients based on a Gaussian scale mixture (GSM) which is the product of a Gaussian random vector and an independent hidden random scalar multiplier. This model can account for both marginal and pairwise joint distributions of wavelet coefficients.

In most of the above statistical models, though the phase holds crucial information about image structures and features [5], only the real part or the magnitude of the transform coefficients is modeled and used for image processing applications. Some previous works employ phase information of the complex wavelet for some applications. The image features such as edges and shadows are determined by analyzing the phase of the harmonic components [6] or computing the phase congruency [7]. Some other applications exploit the local phase information across scales of the complex wavelet such as the description of texture images [8], the detection of blurred images [9] and object recognition [10]. The investigation of local phase in the same orientation and the same scale is based on the dual-tree complex wavelet transform [11] and the complex directional filter bank (CDFB) [12]. Therefore an accurate statistical model of the phase of the complex wavelet coefficients can be beneficial to the developments in the image processing community. In particular, in this paper we propose a model of the phase difference of neighboring complex wavelet coefficients called relative phase (RP), which has been successfully applied in order to classify texture images [12]. In simulations, we show that the proposed model further improves the classification rate.

2. COMPLEX GAUSSIAN MODEL AND PHASE DISTRIBUTION

Our objective in this section is to find a statistical model which is able to accurately capture the phase information in the complex wavelet domain, and is also able to sufficiently describe the natural images.

2.1 Complex Gaussian Distribution

By construction of the complex wavelet, the outputs of the complex filters are the complex coefficients. We assume that the real and imaginary coefficients in each subband are normally distributed. This assumption will be relaxed to cover a much broader class of distributions in the next section. Let $\mathbf{z} = \left(z_1, z_2\right)^T$ be a complex random vector, where z_1 represents the reference coefficient, z_2 represents the neighboring coefficient and $\mathbf{z} = \mathbf{x} + j\mathbf{y}$. Hence, $\mathbf{x} = \left(x_1, x_2\right)^T$ and $\mathbf{y} = \left(y_1, y_2\right)^T$ are two real random vectors normally distributed with a joint density functions $p(\mathbf{x}, \mathbf{y})$. Since the complex directional filters are bandpass, it is clear that $E[z_n] = E[x_n] + jE[y_n] = \mathbf{0}$ and $E[\mathbf{z}\mathbf{z}^T] \approx \mathbf{0}$, where $E[.]$ is the expectation operator and $n = 1, 2$. Furthermore, $\mathbf{C_z} = E[\mathbf{z}\mathbf{z}^H]$ is defined as the complex covariance matrix. In these expressions, the superscript T denotes transposition, the superscript H denotes complex conjugate transposition, and $j = \sqrt{-1}$. By definition, $\mathbf{C_z}$ is positive definite and Hermitian symmetric, hence, its inverse exists. Then $p(\mathbf{x}, \mathbf{y})$ may be written as a function of $\mathbf{z}$ such as $p(\mathbf{x}, \mathbf{y}) \equiv p(\mathbf{z})$, where $p(\mathbf{z})$ is a real-valued function of the complex vector $\mathbf{z}$. The density function $p(\mathbf{z})$ is commonly referred to as the complex Gaussian density function and can be written as [13]

$$p_{\mathbf{z}}(\mathbf{z}) = \frac{\exp\left(-\mathbf{z}^H \mathbf{C_z^{-1}} \mathbf{z}\right)}{\pi^2 \det(\mathbf{C_z})}. \tag{1}$$

2.2 Joint Distribution of Neighboring Phases

From the complex Gaussian model (1), we investigate the behaviors of the joint distribution of neighboring phases in the complex wavelet domain. Let $\mathbf{z} = \mathbf{r}e^{j\mathbf{\Theta}}$, then we can have the joint distribution $p_{\mathbf{r},\mathbf{\Theta}}(\mathbf{r}, \mathbf{\Theta}) = r_1 r_2 p_{\mathbf{z}}(\mathbf{z})$[14] as

$$p_{\mathbf{r},\mathbf{\Theta}}(r_1, r_2, \theta_1, \theta_2) = r_1 r_2 \frac{\exp\left(-\mathbf{z}^H \mathbf{C_z^{-1}} \mathbf{z}\right)}{\pi^2 \det(\mathbf{C_z})}. \tag{2}$$

In each subband, the complex wavelet coefficients have zero mean, and covariance $\mathbf{C_z} = E[\mathbf{z}\mathbf{z}^H] = \begin{bmatrix} \psi_{11} & \psi_{12} \\ \psi_{12}^* & \psi_{22} \end{bmatrix} = \mathbf{\Phi^{-1}}$. The matrix $\mathbf{C_z}$ is a positive definite Hermitian matrix, so its inverse $\mathbf{\Phi}$

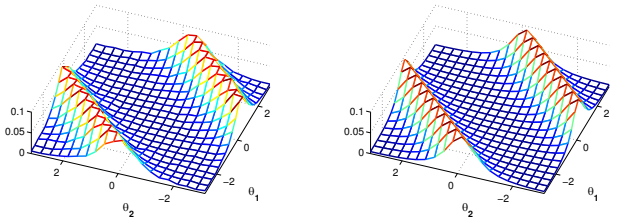

(a) empirical distribution (b) model

Figure 1: The empirical joint distribution of neighboring phases and the joint density function with the parameter values $\mu = 0.15, \lambda = 0.74$ at a particular complex wavelet subband for texture image 'Misc.0002'.

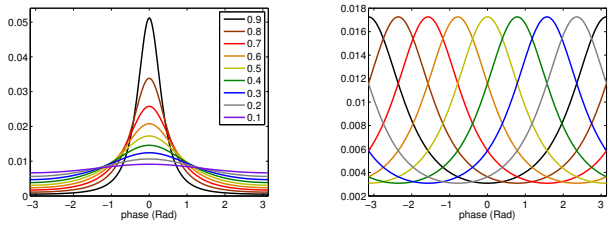

(a) (b)

Figure 2: Distributions of relative phase: (a) $\lambda = [0.1, 0.2, ..., 0.9]$ and $\mu = 0$, (b) $\lambda = 0.5$ and $\mu = [-\pi, -3\pi/4, ..., 3\pi/4]$.

exists. Let $\mathbf{\Phi} = \begin{bmatrix} \varphi_{11} & \varphi_{12} \\ \varphi_{12}^* & \varphi_{22} \end{bmatrix}$, where $\varphi_{12} = |\varphi_{12}|e^{j\mu}$, and the superscript $*$ denotes the complex conjugate. Then $\mathbf{z}^H \mathbf{C_z^{-1}} \mathbf{z} = r_1^2\varphi_{11} + r_2^2\varphi_{22} + 2\mathbf{Re}[r_1 r_2 |\varphi_{12}| e^{j(\theta_1 - \theta_2 - \mu)}]$. Hence the joint distribution of two neighboring phases can be written as

$$\begin{aligned} p_{\mathbf{\Theta}}(\theta_1, \theta_2) &= \pi^{-2} \det(\mathbf{\Phi}) \int_0^\infty \int_0^\infty r_1 r_2 \exp(r_1^2\varphi_{11} + r_2^2\varphi_{22}) \\ &\quad .\exp(-2r_1 r_2 |\varphi_{12}| \cos(\theta_1 - \theta_2 - \mu)) dr_1 dr_2, \\ &= \frac{1-\lambda^2}{4\pi^2(1-c^2)} \left[1 - \frac{c\cos^{-1}(c)}{\sqrt{1-c^2}}\right], \end{aligned} \tag{3}$$

where $c = \lambda cos(\theta_1 - \theta_2 - \mu)$, the correlation coefficient $\lambda = \frac{|\varphi_{12}|}{\sqrt{\varphi_{11}\varphi_{22}}} = \frac{|\psi_{12}|}{\sqrt{\psi_{11}\psi_{22}}}$, $\mu = \angle\varphi_{12} = \angle\psi_{12} + \pi$, and $\angle$ denotes the phase. We can see that the behaviors of the model (3) looks very similar to the empirical joint distribution of neighboring phases as in Fig. 1.

2.3 Distribution of Relative Phase

The relative phase at a spatial location (i, j) within a particular complex subband is defined as the phase difference of neighboring complex wavelet coefficients as follows [12]

$$\begin{aligned} \theta(i,j) &= \angle z(i,j) - \angle z_(i, j+1), \\ \text{or } \theta(i,j) &= \angle z(i,j) - \angle z_(i+1, j), \end{aligned} \tag{4}$$

where $z(i, j)$ is the coefficient at position (i, j). The relative phase can be considered as $\theta = \theta_1 - \theta_2$, where θ_1 is the phase of the reference coefficient at location (i, j) and θ_2 is the phase of the nearest neighbor coefficient at location $(i, j+1)$ or $(i+1, j)$. The joint distribution $p_\Theta(\theta_1, \theta_2)$ is shown in (3). Therefore, the distribution of the relative phase θ is given by

$$p_\theta(\theta) = \int_{-\pi}^{\pi} p_\Theta(\theta + \theta_2, \theta_2) d\theta_2 = \frac{1-\lambda^2}{2\pi(1-c^2)} \left[1 - \frac{c\cos^{-1}(c)}{\sqrt{1-c^2}}\right]. \tag{5}$$

where $c = \lambda cos(\theta - \mu)$, $\lambda = \frac{|\psi_{12}|}{\sqrt{\psi_{11}\psi_{22}}}$ and $\mu = \angle\psi_{12} + \pi$. The density function of the relative phase θ (fRP) in (5) with various values of λ and μ are depicted in Fig. 2.

3. COMPLEX GAUSSIAN SCALE MIXTURE MODEL AND PHASE DISTRIBUTION

In section 2, we proposed the density function in (5) for the relative phase within a particular subband with the assumption that the distribution of the real and imaginary coefficients are Gaussian. However, this assumption is often not realistic. A more widely acceptable model is when these coefficients are Gaussian scale mixture (GSM) distributed developed in [3], which is the product of a real Gaussian random vector and an independent hidden random scalar multiplier. The real wavelet coefficients are linked indirectly by their shared dependency on the hidden multiplier. Hence, the GSM model can describe the shape of real wavelet coefficient distributions and the correlation between neighbor coefficients. In this section, we will derive the density function of the relative phase with assumption that the real coefficients and the imaginary coefficients are modeled by the GSM model.

3.1 Gaussian Scale Mixture for Real Wavelet Coefficients

In [3][15], the coefficients within each local neighborhood around a reference coefficient of a pyramid subband are characterized by the GSM model. Suppose that the random vector $\mathbf{u}$ has a Gaussian distribution, the scalar real variable $\sqrt{v}$ has some distribution on $(0, \infty)$ with a density $p_v(v)$ $(v > 0)$, and $\mathbf{u}$ and v are independent. Let $\mathbf{x} \overset{\Delta}{=} \sqrt{v}\mathbf{u}$ be defined as the scale mixtures of Gaussian distribution with [16]

$$p_{\mathbf{x}}(\mathbf{x}) = \int p(\mathbf{x}|v) p_v(v) dv = \int \frac{\exp\left(\frac{-\mathbf{x}^T (v\mathbf{C_u})^{-1}\mathbf{x}}{2}\right)}{(2\pi)^{\frac{N}{2}} (\det(v\mathbf{C_u}))^{1/2}} p_v(v) dv,$$

where $\mathbf{C_u} = E[\mathbf{u}\mathbf{u}^T]$ is the covariance matrix of $\mathbf{u} = \left(u_1, u_2, ...u_N\right)^T$, and N is the dimensionality of $\mathbf{u}$ and $\mathbf{x}$. The conditional density (on v) of $\mathbf{x}$ is Gaussian, and the variable v is known as the multiplier. In general, the neighborhood may include coefficients from other subbands, as well as from the same subbands. The probability density of the multiplier $p_v(v)$ can be found by using maximum log likelihood approach for estimating a nonparametric $p_v(v)$ from an observed set of M neighborhood vectors [15]

$$\widehat{p}_v(v) = \arg\max_{p_v(v)} \sum_{m=1}^{M} log \int_0^\infty p(\mathbf{x}_m|v) p_v(v) dv. \tag{6}$$

3.2 Complex Gaussian Scale Mixture for Complex Coefficients

The complex directional filters produce real coefficients $\mathbf{x}$ and imaginary coefficients $\mathbf{y}$ which are characterized by a GSM model: $\mathbf{x} \overset{\Delta}{=} \sqrt{v}\mathbf{u_r}$ and $\mathbf{y} \overset{\Delta}{=} \sqrt{v}\mathbf{u_i}$. Then $\mathbf{z} \overset{\Delta}{=} \sqrt{v}\mathbf{u}$, where $\mathbf{z} = \mathbf{x} + j\mathbf{y}$ and $\mathbf{u} = \mathbf{u_r} + j\mathbf{u_i}$. Since the distribution of the real part $\mathbf{x}$ is GSM, $p(\mathbf{x}|v)$ is Gaussian. Similarly for the imaginary part $\mathbf{y}$, $p(\mathbf{y}|v)$ is also Gaussian. Thus from section 2.1, the distribution of complex wavelet coefficients $\mathbf{z}$ will be complex Gaussian when it is conditioned on v as follows

$$p(\mathbf{z}|v) = \frac{\exp\left(-\mathbf{z}^H \mathbf{C}_{\mathbf{z}|v}^{-1} \mathbf{z}\right)}{(\pi)^N \det(\mathbf{C}_{\mathbf{z}|v})}, \tag{7}$$

where the covariance matrix $\mathbf{C}_{\mathbf{z}|v} = v\mathbf{C_u}$, $\mathbf{C_u} = E[\mathbf{u}\mathbf{u}^H]$ is complex covariance matrix of $\mathbf{u}$, and N is the dimensionality of $\mathbf{z}$ and $\mathbf{u}$. The distribution of the vector $\mathbf{u}$ is complex Gaussian and the scalar real variable $\sqrt{v}$ has some distribution on $(0, \infty)$ with a density $p_v(v)$ $(v > 0)$. We refer $\mathbf{z} \overset{\Delta}{=} \sqrt{v}\mathbf{u}$ as the scale mixtures of complex Gaussian distribution as follows

$$p_{\mathbf{z}}(\mathbf{z}) = \int \frac{\exp\left(-\mathbf{z}^H (v\mathbf{C_u})^{-1} \mathbf{z}\right)}{(\pi)^N \det(v\mathbf{C_u})} p_v(v) dv. \tag{8}$$

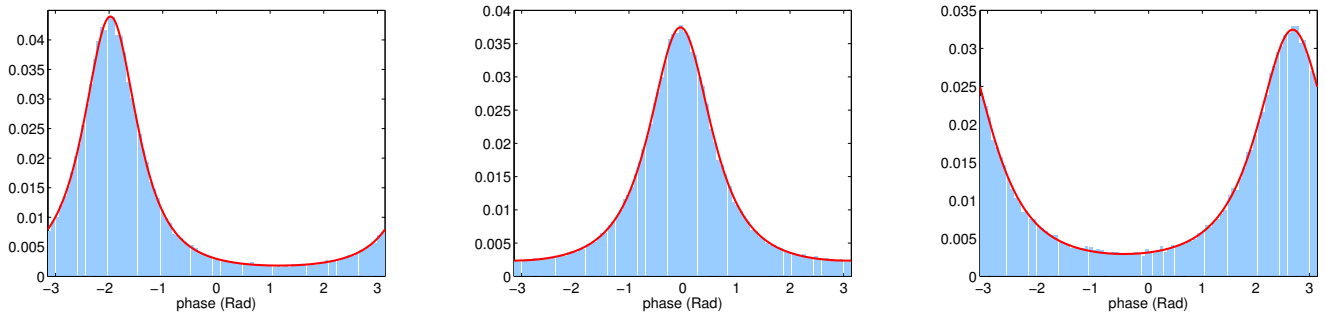

(a) Fabric.0017 $[\mu,\lambda]=[-1.98,0.77]$ $\Delta H/H=0.00018$

(b) Stone.0004 $[\mu,\lambda]=[-0.04,0.71]$ $\Delta H/H=0.00009$

(c) Brick0004 $[\mu,\lambda]=[2.68,0.64]$ $\Delta H/H=0.00023$

Figure 3: Distribution of relative phase fitted to the empirical histograms at a particular finest complex wavelet subband. Below each plot are the estimated parameter values, and the relative entropy ΔH (KLD) between the histogram and the model, as a fraction of the histogram entropy H (with 90 bins).

Similar to the GSM model, the probability density of the multiplier v can be found as in (6).

3.3 Joint Distribution of Neighboring Phases

We have proved that the coefficients $\mathbf{z}=\mathbf{x}+j\mathbf{y}$ within each local neighborhood around a reference coefficient of a complex subband are characterized by a CGSM model. Now we consider the case of $N=2$ with $\mathbf{z}=(z_1,z_2)^T$ and

$$p_{\mathbf{r},\Theta}(r_1,r_2,\theta_1,\theta_2|v)=r_1r_2\frac{\exp\left(-\mathbf{z}^H\mathbf{C}_{\mathbf{z}|v}^{-\mathbf{1}}\mathbf{z}\right)}{(\pi)^2\det(\mathbf{C}_{\mathbf{z}|v})}, \tag{9}$$

where $z_n=r_ne^{j\theta_n}$, $n=1,2$, and covariance $\mathbf{C}_{\mathbf{z}|v}=E[\mathbf{z}\mathbf{z}^H|v]=v\mathbf{C}_{\mathbf{u}}=v\begin{bmatrix}\psi_{11} & \psi_{12}\\ \psi_{12}^* & \psi_{22}\end{bmatrix}=\mathbf{\Phi}^{-\mathbf{1}}$. Hence the joint density of neighboring phases when conditioned on v can be written as

$$\begin{aligned} p_{\Theta}(\theta_1,\theta_2|v) &= \pi^{-2}\det(\mathbf{\Phi})\int_0^\infty\int_0^\infty r_1r_2\exp(r_1^2\varphi_{11}+r_2^2\varphi_{22}) \\ &\quad .\exp(-2r_1r_2|\varphi_{12}|\cos(\theta_1-\theta_2-\mu))dr_1dr_2, \\ &= \frac{1-\lambda^2}{4\pi^2(1-c^2)}\left[1-\frac{c\cos^{-1}(c)}{\sqrt{1-c^2}}\right], \end{aligned} \tag{10}$$

where $c=\lambda cos(\theta_1-\theta_2-\mu)$, $\lambda=\frac{|\varphi_{12}|}{\sqrt{\varphi_{11}\varphi_{22}}}=\frac{|\psi_{12}|}{\sqrt{\psi_{11}\psi_{22}}}$ and $\mu=\angle\varphi_{12}=\angle\psi_{12}+\pi$. We can see that λ and μ are independent from v. Hence

$$\begin{aligned} p_{\Theta}(\theta_1,\theta_2) &= \int p_{\Theta}(\theta_1,\theta_2|v)p_v(v)dv, \\ &= \frac{1-\lambda^2}{4\pi^2(1-c^2)}\left[1-\frac{c\cos^{-1}(c)}{\sqrt{1-c^2}}\right]. \end{aligned} \tag{11}$$

3.4 Distribution of Relative Phase

When the coefficients of a complex subband are characterized by a complex Gaussian or a CGSM model, the joint distribution of neighboring phases in (3) and in (11) are identical. So the distribution of the relative phase shown in (5) is also true with the assumption of CGSM model, where $c=\lambda cos(\theta-\mu)$, $\lambda=\frac{|\psi_{12}|}{\sqrt{\psi_{11}\psi_{22}}}$, $\mu=\angle\psi_{12}+\pi$ and ψ_{ij} are the components of the covariance matrix $\mathbf{C}_{\mathbf{u}}$.

The fRP distribution in (5) fits well with the distribution of the RPs in complex subbands. Fig. 3 shows an empirical histogram of RP in a particular complex wavelet subband for three different images, along with the best fitting of the fRP distribution. Fitting was performed by minimizing the difference between the empirical histogram and the fRP $p_\theta(\theta;\mu,\lambda)$. It should be noted that the parameter μ can be estimated by the mean direction as defined in [12].

Table 1: $\Delta H/H$.

Texture (Vistex)	Subbands	Subband Size	Bins	Ave of $\Delta H/H$
640 subimages	3840	64×64	32	0.0021
40 subimages	240	128×128	64	0.0011
40 images	240	256×256	128	0.0007
Lena	6	256×256	128	0.0008
Barbara	6	256×256	128	0.0029
Boat	6	256×256	128	0.0016
Fingerprint	6	256×256	128	0.0003

We also show the relative entropy ΔH (KLD) between the histogram and the model divided by the histogram entropy H in Table 1. It is clear that fRP fits very well in the 40 Vistex textures with the size of 256×256, the Lena and Fingerprint images with the average of $\Delta H/H=0.0007,0.0008$ and 0.0003 respectively. For other images in Table 1, the performance of the fitted model is still acceptable with $\Delta H/H<0.003$.

4. APPLICATIONS

In this section, the relative phase distribution model is applied to texture image retrieval. A comparison of various features such as energy feature [17], GGD-based feature [18], RP feature [12], our fRP-based feature, and the combination of these features using curvelet transform in texture retrieval is presented. We also include two other multiresolution directional decompositions in feature extraction, namely Gabor decomposition [17] and CDFB [12]. The latter is very similar to the curvelet transform in terms of directionality of the filters and one-sided supports in the frequency domain.

4.1 An Implementation of The Curvelet Transform

Our modified multiresolution and multidirectional discrete transform borrows the ideas from the two recently introduced discrete transforms, which are the pyramidal dual-tree directional filter bank (PDTDFB) [19] and the fast discrete curvelet transform [20]. We define in the frequency plane a set of N 2-D directional filters $\phi_i(\boldsymbol{\omega}),i=1,..,N$ and a lowpass filter $\phi_0(\boldsymbol{\omega})$ in such a way that the directional subbands and the lowpass subband can be decimated without aliasing. The decimation ratio for the lowpass band is $diag\{2,2\}$, and the decimation ratios for the first and second $N/2$ directional filters are $diag\{M/2,2\}$ and $diag\{2,M/2\}$, respectively, where M is a power of two number and is linearly proportional to N. The defined filters in the frequency domain are real-valued functions and satisfy the perfect reconstruction conditions, taking into account the decimation ratio: $\frac{1}{4}\phi_0^2(\boldsymbol{\omega})+\frac{1}{2M}\sum_{j=1}^{N}\phi_j^2(\boldsymbol{\omega})+$

$\phi_j^2(-\omega) = 1$.

Similar to the PDTDFB, our directional filters have one-sided support in the frequency domain, making the subband coefficients complex. The same transform with different values of M and N is applied iteratively at the lowpass subband to create a multiresolution decomposition. In the reconstruction procedure, the final complex components are simply discarded. We can interpret this as a dual-tree FB structure [21]. Our discrete transform also has some similarities to the wrapping-based fast discrete curvelet transform (FDCT) [20] in the sense that both are defined based on windowing in the DFT domain. The main difference is that in the wrapping-based FDCT, the redundancy of the transform is reduced by wrapping the frequency domain of the subbands, while in our implementation, the redundancy is reduced by decimating the subbands by diagonal integer matrices. By this construction, our curvelet basis functions are located on a uniform integer grid at each resolution, while the basis of the FDCT is located on a non-integer grid. For detailed construction of this new directional transform, the reader is referred to [22].

4.2 Texture Feature Extraction

Each image in the database is decomposed by the following three decompositions: the curvelet, the 2-D Gabor transform and the CDFB. The Gabor wavelet and the curvelet are applied with four scales and six orientations per scale, while the CDFB has three scales of eight orientations. For each subband, the mean and standard deviation of the absolute values of the coefficients are calculated as in [17]. The RP feature which includes circular means and standard deviations of the relative phase are computed as in [12] and the GGD features are estimated as in [18]. To construct the fRP based feature vector, the RP matrix of each complex subband in the curvelet domain is created as in (4). For each RP matrix, the two parameters μ and λ of the fRP model are estimated by fitting the RP histogram and the fRP density function (5). These parameters are used to form the fRP model based feature vector.

For the first experiments (results shown in Table 2), the feature vectors are formed from the six subbands at the finest scale of the curvelet transform. The length of the Mag, GGD, RP, fRP feature vectors is twelve because each subband is represented by two parameters. Since the magnitude and phase are combined, the length of the Mag-RP or GGD-fRP feature vector is twenty four. The weighting is needed when we combined the GGD and the fRP feature vector.

In the second experiment (results shown in Table 3), in order to obtain a feature vector which has the same dimension as that of the Gabor [17] and the CDFB-RP [12], the GGD-fRP feature vector is formed by twelve features of the fRP model from the finest scale, twenty-four features of the GGD model from the two finest scales, and twelve means of the magnitudes of the curvelet coefficients from the two coarsest scales. For each kind of features, the weighting is needed to get the best performance.

4.3 Texture Image Database and Feature Database

We select 40 image textures from the VisTex databases used in [18] for our experiments. Each of these 512×512 images is divided into sixteen 128×128 non-overlapping sub-images, thus creating a database of 640 texture samples. Each original image is treated as a single class and therefore there are 16 samples from each of the 40 classes. To reduce the intensity correlation, all images are normalized to have zero mean and unit variance. For each image in the database, the curvelet transform is applied. The RP matrix of each subband is created as in (4), and their corresponding feature vectors are computed.

4.4 Distance Measure and Query Processing

The query pattern can be any one of the texture patterns from the image database. The distance between two magnitude feature vectors and two RP feature vectors are computed as in [12] and the distance between two GGD feature vectors is computed as in [18]. The distance between two fRP feature vectors f_x and f_y is given by

$$d(f_x, f_y) = \sum_k D_{KL}(p(.;\mu_k(x), \nu_k(x)) || p(.;\mu_k(y), \nu_k(y))),$$

where k is the index of the subbands and the Kullback-Leibler divergence D_{KL} between the two PDFs $p(\theta;\mu_1,\lambda_1)$ and $p(\theta;\mu_2,\lambda_2)$ is defined as

$$D_{KL}(P_1||P_2) = \int_{-\pi}^{\pi} p(\theta;\mu_1,\lambda_1) \log \frac{p(\theta;\mu_1,\lambda_1)}{p(\theta;\mu_2,\lambda_2)} d\theta. \qquad (12)$$

For each query image, N nearest neighbors are selected, and the number of these textures belonging to the same class as the query texture, except for itself, is counted. This number (less than or equal to fifteen) divided by fifteen is defined as the retrieval rate. The performance of the entire class is obtained by averaging this rate over the sixteen members which belong to the same class of texture. The average of all classes is the overall performance of the method.

Table 2: Average Retrieval Accuracy of 40 VisTex Texture Images Using Curvelet Transform with Various Features Extracted from Six Subbands at the Finest Scale. (Mag denotes the magnitude feature.)

	Mag	**GGD**	**RP**	**fRP**	**Mag-RP**	**GGD-fRP**
Feature Type	m,σ	α,β	m_c,σ_c	μ,λ	m,σ m_c,σ_c	$\alpha,\beta,$ μ,λ
Feature Length	12	12	12	12	24	24
N = 15	62.07	64.64	60.29	67.68	74.68	**78.95**

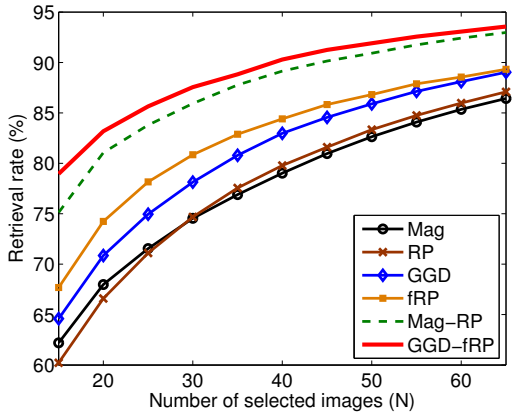

Figure 4: Average retrieval rate according to the number of top images considered when the database is 40 VisTex textures. The curvelet transform with various features extracted from the six subbands at the finest scale are used.

4.5 Experimental Results

Table 2 summarizes the overall retrieval rates using the curvelet transform with various features extracted from the finest subbands. If only the top 15 texture images that are nearest to the query texture are considered, and only 12 features are used, the fRP feature and the GGD feature give the best overall retrieval performances of 67.68 % and 64.64 %, while the magnitude and RP features are at 62.07 %, and 60.29 %, respectively. Fig. 4 shows the overall performances for the case of N from 15 to 65. It is clear that the feature vector based on the fRP model is consistently better than the magnitude feature and the RP feature. This confirms that the behavior of the RPs is captured accurately by the fRP distribution even with a small number of samples. When the magnitude and phase information are combined, the overall retrieval accuracy of the GGD-fRP

Table 3: Average Retrieval Accuracy of 40 VisTex Texture Images Using Various Features.

	Gabor	**Cur-GGD**	**CDFB-RP**	**GGD-fRP**
Feature type	m, σ	α, β m, σ	m, σ m_c, σ_c	$\alpha, \beta,$ μ, λ, m
Feature length	48	48	48	48
N = 15	80.81	81.52	82.26	**85.82**

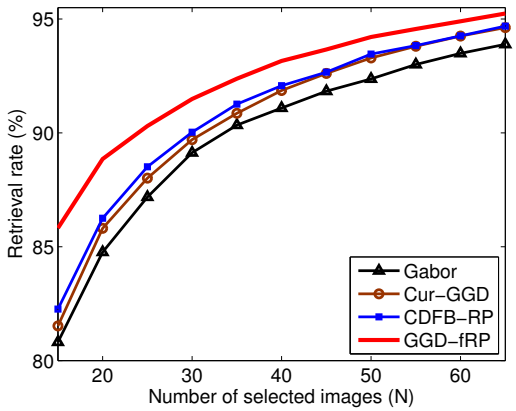

Figure 5: Average retrieval rate according to the number of top images considered when various features are used.

feature is also higher than the Mag-RP feature which is formed by the magnitude and the RP features (m_c and σ_c) as proposed in [12] for the case of $N = 15$ as shown in Table 2.

In the second experiment, we compare our proposed GGD-fRP feature using the modified discrete curvelet transform with the Gabor and CDFB. In this experiment, all twenty four subbands are used to form feature vectors. If only the top 15 texture images nearest to the query texture are considered, the GGD-fRP gives the best overall retrieval performance of 85.82 % as shown in Table 3. The CDFB-RP [12] and the GGD [18] are at 82.26 % and 81.52 %, while the magnitude based Gabor [17] is at 80.81 %. Fig. 5 shows the overall performances of the GGD-fRP model is consistently better than the others for the case of N from 15 to 65. It is clear that the information gained from the fRP phase model raises the performance of the GGD-fRP significantly higher than those of other features.

5. CONCLUSION

A new statistical model is proposed for modeling the phase distribution in the transform domain. From the experiments, the fRP distribution captures the behaviors of RPs in the complex directional wavelet subbands of different natural images. Moreover, a new image feature based on the fRP model is proposed for texture image retrieval application. The fRP model describes nicely the directional information from the texture images because higher image retrieval accuracy is achieved by using the fRP model instead of using the magnitude [17] or the RP parameters [12]. In addition to the GGD model of real coefficients typically used in other feature extraction methods [18], the fRP-based phase information is incorporated to further improve the performance.

REFERENCES

[1] S.G. Malat, *A wavelet tour of signal processing*, San Diego: Academic Press, 1998.

[2] M. Course, R.D. Nowak, and R.G. Baraniuk, "Wavelet-based signal processing using hidden Markov models," *IEEE Trans. Signal Processing. (Special Issue on Wavelet and Filter banks)*, pp. 886–902, Apr 1998.

[3] M.J. Wainwright and E.P. Simoncelli, "Scale mixtures of Gaussians and the statistics of natural images," *Adv. Neural Information Processing Systems*, vol. 12, 2000.

[4] L. Sendur and I.W. Selesnick, "Bivariate shrinkage functions for wavelet-based denoising exploiting interscale dependency," *IEEE Trans. on Signal Processing*, vol. 50, no. 11, Nov 2002.

[5] A.V. Oppenheim and J.S. Lim, "The importance of phase in signals," in *Proc. of the IEEE*, 1981, vol. 69, pp. 529–541.

[6] M.C. Morrone and R.A. Owens, "Feature detection from local energy," *Pattern Recognition Letters*, vol. 6, no. 5, pp. 303 – 313, Dec 1987.

[7] P. Kovesi, "Image features from phase congruency," *Videre: A Journal of Computer Vision Research*, vol. 1, no. 3, pp. 2–26, Summer 1999.

[8] J. Portilla and E.P. Simoncelli, "A parametric texture model based on joint statistics of complex wavelet coefficients," *Int'l Journal of Computer Vision*, vol. 40, no. 1, pp. 49–71, Oct 2000.

[9] Z. Wang and E.P. Simoncelli, "Local phase coherence and the perception of blur," in *Advances in Neural Information Processing Systems*, MIT Press, Ed., May 2004, vol. 16.

[10] R. Anderson, N. Kingsbury, and J. Fauqueur, "Coarse-level object recognition using interlevel products of complex wavelets," in *Proc. ICIP*, Sept 2005, vol. 1.

[11] R. Anderson, N. Kingsbury, and J. Fauqueur, "Determining multiscale image feature angles from complex wavelet phases," in *Proc. ICIAR*, Sept 2005.

[12] A.P.N. Vo, S. Oraintara, and T.T. Nguyen, "Using phase and magnitude information of the complex directional filter bank for texture image retrieval," in *Proc. ICIP*, Sept 2007.

[13] N.R. Woodman, "Statiscal analysis based on a certain multivariate complex Gaussian distribution," *Annals Math. Statist.*, vol. 34, pp. 152–177, 1963.

[14] K.S. Miller, "Complex Gaussian processes," *SIAM Rev.*, vol. 11, pp. 544–567, 1969.

[15] J. Portila, V. Strela, M.J. Wainwright, and E.P. Simoncelli, "Image denoising using scale mixtures of Gaussians in the wavelet domain," *IEEE Trans. Image Processing*, vol. 12, no. 11, Nov 2003.

[16] D.F. Andrews and C.L. Mallows, "Scale mixtures of normal distributions," *Journal of the Royal Statistical Society*, vol. 36, pp. 99–102, 1974.

[17] B.S. Manjunath and W.Y. Ma, "Texture features for browsing and retrieval of image data," *IEEE Trans. on PAMI*, vol. 18, no. 8, pp. 837–42, Aug 1996.

[18] M.N. Do and M. Vetterli, "Wavelet-based texture retrieval using generalized Gaussian density and Kullback-Leibler distance," *IEEE Trans. on Image Processing*, vol. 11, pp. 146–158, Dec. 2002.

[19] T.T. Nguyen and S. Oraintara, "A shift-invariant multiscale multidirection image decomposition," in *Proc. ICASSP'06*, France, May 2006, pp. 153–156.

[20] E.J. Candes, L. Demanet, D.L. Donoho, and L. Ying, "Fast discrete curvelet transforms," *Multiscale Modeling Simulation*, vol. 5, no. 3, pp. 861–899, 2006.

[21] N.G. Kingsbury, "Complex wavelets for shift invariant analysis and filtering of signals," *Journal of Applied and Computaional Harmonic Analysis*, vol. 10, no. 3, 2001.

[22] T.T. Nguyen and H. Chauris, "Uniform discrete curvelet transform," *Submitted for publication in the IEEE Trans. on Image Processing*, Jan 2008.